Author/s:
Porter, LH;Bakshi, A;Pook, D;Clark, A;Clouston, D;Kourambas, J;Goode, DL;Risbridger, GP;Taylor, RA;Lawrence, MG

Title:
Androgen receptor enhancer amplification in matched patient-derived xenografts of primary and castrate-resistant prostate cancer

Date:
2021-06-01

Citation:
Porter, L. H., Bakshi, A., Pook, D., Clark, A., Clouston, D., Kourambas, J., Goode, D. L., Risbridger, G. P., Taylor, R. A. & Lawrence, M. G. (2021). Androgen receptor enhancer amplification in matched patient-derived xenografts of primary and castrate-resistant prostate cancer. Journal of Pathology, 254 (2), pp.121-134. https://doi.org/10.1002/path.5652.

Lawrence Mitchell (Orcid ID: 0000-0001-9520-3000)
Taylor Renea (Orcid ID: 0000-0003-2609-2380)

20-843.R1 **Poulsom-EDITED UK English** **ORIGINAL ARTICLE**

Androgen receptor enhancer amplification in matched patient-derived xenografts of primary and castrate-resistant prostate cancer

Laura H. Porter[1,†], Andrew Bakshi[1, 2,†], David Pook[1, 3], Ashlee Clark[1], David Clouston[4], John Kourambas[5], MURAL Investigators[1, 6], David L. Goode[2, 7, 8,#], Gail P. Risbridger[1, 7, 8,#], Renea A. Taylor[7, 8, 9,# *], Mitchell G. Lawrence[1, 7, 8,# *]

1. Monash Partners Comprehensive Cancer Consortium, Monash Biomedicine Discovery Institute Cancer Program, Prostate Cancer Research Group, Department of Anatomy and Developmental Biology, Monash University, Clayton, VIC 3800, Australia
2. Computational Cancer Biology Program, Peter MacCallum Cancer Centre, Melbourne, VIC 3000, Australia
3. Medical Oncology, Monash Health, Clayton, VIC 3168, Australia
4. TissuPath, Mount Waverley, VIC 3149, Australia
5. Department of Medicine, Monash Health, Casey Hospital, Berwick, VIC 3806, Australia
6. Melbourne Urological Research Alliance (MURAL), Biomedicine Discovery Institute Cancer Program, Department of Anatomy and Developmental Biology, Monash University, Clayton, VIC 3800, Australia
7. Peter MacCallum Cancer Centre, Melbourne, VIC 3000, Australia
8. Sir Peter MacCallum Department of Oncology, University of Melbourne, Parkville, VIC 3010, Australia
9. Monash Partners Comprehensive Cancer Consortium, Monash Biomedicine Discovery Institute Cancer Program, Prostate Cancer Research Group, Department of Physiology, Monash University, Clayton, VIC 3800, Australia

†Equal first authors

[#]Contributed equally

***Correspondence to:** RA Taylor**,** Monash Biomedicine Discovery Institute Cancer Program, Department of Physiology, Monash University, Level 3, Building 76, 19 Innovation Walk, Clayton, VIC, 3800, Australia. E-mail: renea.taylor@monash.edu or MG Lawrence, Monash Biomedicine Discovery Institute Cancer Program, Department of Anatomy and Developmental Biology, Monash University, Level 3, Building 76, 19 Innovation Walk, Clayton, VIC, 3800, Australia. E-mail: mitchell.lawrence@monash.edu

Running Title: Xenograft models of AR enhancer amplifications

Word count: ~4600

This is the author manuscript accepted for publication and has undergone full peer review but has not been through the copyediting, typesetting, pagination and proofreading process, which may lead to differences between this version and the Version of Record. Please cite this article as doi: 10.1002/path.5652

Conflicts of interest:

D Pook (Honoraria: Astellas, Ipsen, Novartis; Advisory/Consulting: Pfizer, Merck Sharp & Dohme, Bristol-Myers Squibb; Research Funding to institution: Medivation, Bristol-Myers Squibb, Merck Sharp & Dohme, Exelixis, Pfizer, Astellas, Bayer, SymVivo, Amgen; Travel: Bristol-Myers Squibb, Pfizer, Amgen); G Risbridger, R Taylor and M Lawrence (Provision of reagents for laboratory research: Zenith Epigenetics; Other research collaborations: Pfizer, Astellas). All remaining authors declared no conflicts of interest.

Abstract

Amplifications of the androgen receptor (AR) occur in up to 80% of men with castration-resistant prostate cancer (CRPC). Recent studies highlighted that these amplifications not only span the *AR* gene, but usually encompass a distal enhancer. This represents a newly recognised, non-coding mechanism of resistance to AR-directed therapies, including enzalutamide. To study disease progression before and after *AR* amplification, we used tumour samples from a castrate-sensitive primary tumour and castrate-resistant metastasis of the same patient. For subsequent functional and genomic studies, we established serially transplantable patient-derived xenografts (PDXs). Whole genome sequencing showed that alterations associated with poor prognosis, such as *TP53* and *PTEN* loss, existed before androgen deprivation therapy, followed by co-amplification of the *AR* gene and enhancer after the development of metastatic CRPC. The PDX of the primary tumour, without the *AR* amplification, was sensitive to AR-directed treatments, including castration, enzalutamide, and apalutamide. The PDX of the metastasis, with the *AR* amplification, had higher *AR* and *AR-V7* expression in castrate conditions, and was resistant to castration, apalutamide, and enzalutamide *in vivo*. Treatment with a BET inhibitor outperformed the AR-directed therapies for the metastasis, resulting in tumour regression for some, but not all, grafts. Therefore, this study provides novel matched PDXs to test potential treatments that target the over-abundance of AR in tumours with *AR* enhancer amplifications.

Keywords:

Patient-derived xenograft, castration-resistant prostate cancer, androgen receptor, enhancer, intraductal carcinoma of the prostate, BET inhibitor

Introduction

The androgen receptor (AR) controls the identity of prostate epithelial cells. In benign prostate tissue, it suppresses growth and promotes differentiation of luminal epithelium; but, in prostate cancer, it stimulates growth and promotes tumour progression [1]. The evolving, pivotal role of the AR in prostate epithelium has been described as “lineage addiction” or “oncogene addiction” [2,3]. This makes the AR the main therapeutic target for advanced prostate cancer, with androgen deprivation therapy and potent AR-directed treatments used to block AR function, either alone or in combination with other treatments [4].

Inevitably, prostate cancer cells develop resistance to AR-directed treatments. With the exception of tumours that transdifferentiate to AR-null phenotypes, such as neuroendocrine prostate cancer [5,6], most castration-resistant prostate cancers (CRPC) remain reliant on AR signalling [7,8]. This is often through the positive selection of cells with aberrations in the AR pathway, including mutations and structural rearrangements of the *AR* gene, expression of AR variants, intracrine androgen synthesis, and changes in the expression of AR cofactors, despite ongoing AR-targeted treatments [9].

Amplifications of the *AR* locus, which result in increased AR expression, are another prominent mechanism of castration resistance [10,11]. Based on recent whole genome sequencing studies, these amplifications often extend beyond the coding region to encompass an enhancer, which is located approximately 650 kilobases upstream of *AR* and activated in CRPC [8,12,13]. The *AR* gene and enhancer can be amplified separately or together [8,12,14], and these alterations are detected in up to 80% of patients with CRPC [8,12]. Notably, *AR* gene and enhancer amplifications are associated with decreased sensitivity to AR-directed treatments in cell lines and patients, as well as poorer progression-free and overall survival [13–15].

The prevalence of *AR* amplifications in CRPC raises the question of how to treat these tumours more effectively. Unfortunately, the paucity of preclinical models that represent contemporary treatment of CRPC make it more challenging to resolve this question. Through the Melbourne Urological Research Alliance (MURAL), we have been establishing new patient-derived models to reflect the spectrum of mechanisms of castration-resistance [16,17]. Here we report a case study of a new, matched pair of serially transplantable patient-derived xenografts (PDXs) of castrate-sensitive and castrate-resistant prostate cancer from a patient treated with chemo-hormonal therapy. With these tumours, we document the emergence of an *AR* gene and enhancer amplification, which drives increased AR expression and resistance to AR-directed treatments.

Materials and methods

See Supplementary materials and methods for further details of all experiments.

Patient specimens and patient-derived xenografts

Patient tissue was collected according to human ethics approvals from Monash University (2004/145), Cabrini Hospital (03-14-04-08), and Eastern Health (E55/1213). Serially-transplantable xenografts were established by the Monash Urological Research Alliance (MURAL) in accordance with Monash University animal ethics approvals (MARP 2012/158, MARP 2014/085, 17963 and 22185) [16]. For castration experiments, PDXs were regrafted under the renal capsule (short-term experiments) or subcutaneously (long-term experiments) before mice were castrated and testosterone pellets removed. For *in vivo* drug treatments, grafts from PDX-167.2M were established subcutaneously in castrated mice. Mice were treated for 28 days with either vehicle, 10 mg/kg enzalutamide, 10 mg/kg apalutamide, 10 mg/kg docetaxel, 50 mg/kg carboplatin, 0.33

mg/kg talazoparib (all from Selleck Chemicals, Houston, TX, USA) or 50 mg/kg ZEN-3694 (Zenith Epigenetics, Calgary, AB, Canada).

In vitro drug testing

Explant and organoid experiments were performed as described previously [16]. Explants were treated for 48 h and immunohistochemistry was performed using antibodies listed in **supplementary material, Table S1**. Staining was scored using Aperio ImageScope software (Leica Biosystems, Mount Waverley, VIC, Australia). Organoids were treated for four days with enzalutamide at specified concentrations.

DNA and RNA analysis

All DNA and RNA sequencing data are available from the Sequence Read Archive BioProject ID PRJNA681493. Low-coverage whole genome sequencing of formalin-fixed, macro-dissected tissue was performed using an Illumina NovaSeq 6000 S1 System (Illumina, Scoresby, VIC, Australia; 150 bp paired end). Copy-number profiles were constructed using Control-FREEC [18] and a phylogenetic tree was constructed with the R package ape (5.2)[19]. Whole genome sequencing was performed using an Illumina HiSeqX (Illumina; 150 bp paired end). A curated set of genes frequently altered in prostate cancer [11,20] was used to highlight major alterations (**supplementary material, Table S2**).

RNA sequencing with Illumina NEBNext Ultra TM II Directional libraries was performed on NextSeq500 (Illumina; paired-end 75 bp). Xenomapper was used to remove mouse reads [21]. Single sample gene set enrichment analysis [22] was used to calculate the enrichment of MSigDB50 pathways and AR-regulated signatures [23–25]. *AR* mRNA

transcript abundance was compared across PDXs and patient tissues using normalised (copies per million) RNAseq data (Lexogen 3' Quantseq FWD (Lexogen, Vienna, Austria) and Illumina HiSeq 2000/2500). Reverse Transcription-quantitative PCR (RT-qPCR) for *AR-FL, AR-V7* and *AR-V9* was performed using primers listed in **supplementary material, Table S3** [26].

Statistical analyses

Linear mixed model analyses were conducted using SPSS Statistics (Version 25; International Business Machines Corporation, Armonk, NY, USA). All other statistical analyses were conducted using GraphPad Prism 7 software (GraphPad Software Inc, La Jolla, CA, USA). Tests were two-tailed and are listed in figure legends. Statistical significance was set at $P < 0.05$.

Results

Establishing new patient-matched models of castrate-sensitive and castrate-resistant prostate cancer

To generate new PDX models of prostate cancer, we consented patients undergoing radical prostatectomy for high grade group primary prostate cancer and tracked their clinical progression to identify tumours that rapidly metastasised and failed systemic treatments. This approach produced PDX-167.1R, established from the primary tumour of a patient with high-risk prostate cancer (**Figure 1A, supplementary material, Figure S1A**). Nineteen months following radical prostatectomy, the same patient underwent palliative surgery to remove a dural metastasis of the spinal cord. From this castrate-resistant metastasis, we established PDX-167.2M (**Figure 1A**). Both PDXs were serially transplantable, with the PDX from the metastasis growing faster than the PDX from the primary tumour (**Figure 1B**). Pathology review and immunohistochemical staining for prostate cancer biomarkers showed that both PDXs maintained the histopathology of the original patient specimens across multiple generations (**Figure 1C**).

Patient 167 had rapid clinical progression, going from diagnosis to death within 31 months (**Figure 1D**). The patient had a radical prostatectomy to remove the primary tumour and was treatment-naïve prior to surgery. The primary tumour had several traits of locally advanced high-risk prostate cancer. The index lesion was grade group 5 (Gleason 4+5) acinar adenocarcinoma with large cribriform architecture and multiple regions of intraductal carcinoma of the prostate (IDC-P), a growth pattern that is prevalent in high-risk disease [27]. Furthermore, this large volume tumour (34.1 cc) was stage pT3b, with extensive invasion into the lymphovasculature, perineural space, seminal vesicles, and bladder neck (**supplementary material, Figure S1A,B**). There were positive margins after surgery, and although no lymph node metastases were

identified, a small metastatic nodule was resected from the anterior prostatic fat (**supplementary material, Figure S1A**). Therefore, the grade, stage, size, subpathologies and local metastatic deposits all indicated that this was a high-risk primary tumour.

After failing salvage radiation therapy, the patient received combination treatment with ADT and six cycles of docetaxel, according to the CHAARTED and STAMPEDE protocols [28,29]. However, he developed CRPC with a spinal cord metastasis, which was surgically removed to reduce pressure on the spinal cord (**Figure 1D**). This tissue was grown as PDX-167.2M (**Figure 1B**). After surgery and the collection of tissue for PDX-167.2M, the patient received further systemic treatments. He had a temporary response to cabazitaxel, but no response to enzalutamide, before dying from CRPC less than three years after diagnosis (**Figure 1D**).

Progressive molecular changes between the matched PDXs are associated with advanced prostate cancer

To compare the genomic features across the primary prostate tumour and the PDXs, we performed low coverage whole genome sequencing on 14 spatially-distinct regions within the index tumour, a region from the non-index tumour, benign prostate tissue, and the local metastatic nodule (**Figure 2A**). The pattern of copy number alterations across regions of the index tumour showed that they arose from a common tumour clone, rather than genomically distinct foci (**Figure 2B**). Tumour regions containing different growth patterns of adenocarcinoma, including cribriform architecture and IDC-P, were interspersed in hierarchical clustering (**Figure 2B**), consistent with a common genomic origin [30]. The spatially separate low grade non-index tumour had a low number of

CNAs; it shared some CNAs with the index tumour but lacked others that were common to the index tumour and metastases (**Figure 2C**).

The low coverage whole genome sequencing data did not identify a specific region as the definitive source of metastatic cells. Nevertheless, regions 2 and 12 of the index tumour clustered most closely with the local metastasis and spinal metastasis (PDX-167.2M) (**Figure 2B**). Fortuitously, PDX-167.1R was established from tissue adjacent to region 12 and had a very similar pattern of CNAs to this region (**Figure 2B,C**).

There were numerous shared somatic copy number alterations across the primary tumour, including CNAs that are commonly observed in prostate cancer, such as gain of 8q, loss of 6q, 8p and loss of chromosome 18 (**Figure 2C, supplementary material, Figure S2A and Table S4**) [31–33]. For example, loss of 8p was detected in every region of the index tumour (**Figure 2C, supplementary material, Figure S2A**). These CNAs contributed to the high percentage of genome alteration (PGA) across the index tumour (average 12.5%, range 3–33%; **Figure 2D**), comparable to the 74th percentile of PGA in a cohort of 680 cases of localised prostate cancer (**supplementary material, Figure S2B**) [20]. High PGA is a marker of poor prognosis [34], so this is further evidence that Patient 167 had a high-risk tumour. PGA further increased in the spinal metastasis (PDX-167.2M; **Figure 2D**), consistent with metastases in public cohorts (**supplementary material, Figure S2B**) [20,35].

To compare the other features of the matched PDXs in more detail, we performed deeper coverage (45x) whole genome sequencing (WGS) and RNA sequencing. No pathogenic germline mutations were detected (**supplementary material, Figure S2C**). There were progressive genomic changes from the primary tumour to the metastasis, including more copy number alterations and a genome doubling in PDX-167.2M versus PDX-167.1R (**Figure 2E, supplementary material, Figure S2D, and Tables S5–8**). Both tumours

had extensive intra- and inter-chromosomal rearrangements (**supplementary material, Figure S2E**), and a focal homozygous deletion of the 3' end of *PTEN* (**supplementary material, Figure S2F**). Both PDXs also had a missense mutation of *TP53* (G244C) and loss of the second, wild-type allele (**Figure 2F**). This loss-of-function mutation lies in the DNA binding domain of p53 [36]. It was a dominant feature of the tumour, since it occurred at high allele frequency in the PDXs (95%) and was even detected in four different samples of the primary index tumour in low coverage whole genome sequencing (**supplementary material, Table S4**).

Other notable alterations included a gain of the *AR* in the metastasis, and LOH of *APC* in PDX-167.1R, followed by an inactivating frameshift mutation of the remaining allele in PDX-167.2M (**Figure 2F**). In addition, despite LOH of *CCND1* in PDX-167.1R, it was the most highly amplified gene in the metastasis (**Figure 2F**).

We also identified progressive transcriptomic changes from the primary tumour to the metastasis using single sample gene set enrichment analysis of RNAseq data [22]. Several hallmark pathways associated with proliferation (e.g. mitotic spindle, E2F targets, and G2M checkpoints) were more highly expressed in the metastasis (**supplementary material, Figure 3**), consistent with faster growth rate of PDX-167.2M and its amplification of *CCND1* (**Figure 1B, Figure 2F**).

To understand how the tumours from Patient 167 fit in the broader context of prostate cancer, we compared their genomic features to large patient cohorts. PDX-167.1R did not belong to any of the molecular classes of primary prostate cancer from TCGA, since it lacked the defining driver alterations (*ERG*, *ETV1*, *ETV4* and *FL1* fusions and mutations in *SPOP*, *FOXA1* and *IDH1*) [32]. Instead, it shared similarities with the ~26% of tumours that fall outside the molecular subclasses, including the high burden of CNAs and *TP53* mutation. Compared to Armenia and colleagues' aggregated cohort of prostate

cancer, PDX-167.2M shared five of the most common alterations that are enriched in metastases versus primary tumours (*AR* and *CCND1* amplification, *PTEN*, *TP53* and *APC* loss) [20].

Overall, these genomic and transcriptomic data show that the high-risk primary tumour accumulated poor prognostic features as it progressed to metastatic CRPC, including increased PGA; genome doubling; *PTEN*, *TP53* and *APC* loss; *AR* and *CCND1* gain; and proliferative gene expression signatures. Therefore, PDX-167.1R and -167.2M provide matched models to study the progression of prostate cancer in the context of several common alterations.

Matched PDXs maintain responses to androgen deprivation *in vivo*

To compare the reliance of the matched PDXs on the AR pathway, we used *in vivo* castration studies. The levels of circulating androgens in castrated mice are akin to those in patients treated with abiraterone acetate [37]. We initially performed short-term castration studies with the grafts implanted under the renal capsule. For PDX-167.1R, castration caused a rapid decrease in tumour volume and the percentage of proliferating tumour cells, marked by Ki67 staining, which was sustained for three weeks after castration (**Figure 3A,B**). Therefore, PDX-167.1R was castrate-sensitive, consistent with it being established from hormone-naïve primary prostate cancer. In contrast, PDX-167.2M did not regress after castration (**Figure 3C**), as expected given that it was established from a castrate-resistant metastasis. Yet, in testosterone-supplemented mice, PDX-167.2M grew larger and had higher Ki67 staining (**Figure 3C,D**), showing that it remained androgen-responsive. We verified these observations with long-term castration experiments where grafts were established subcutaneously to monitor tumour growth over time. After castration, grafts from PDX-167.1R regressed and remained small in volume for up to 150 days in castrated mice (**Figure 3E**). In comparison, after

castration there was a delay in the growth of PDX-167.2M grafts, and temporary regression, before they resumed rapid tumour growth (**Figure 3E**). PDX-167.2M was also serially transplantable in castrated mice (**Figure 3F**). Therefore, matched PDXs maintain responses to castration *in vivo* and can be used to model castrate-sensitive and castrate-resistant disease respectively.

Castration-resistance of PDX-167.2M is associated with a genomic amplification of the *AR* and enhancer

To investigate the mechanisms of castration-resistance in PDX-167.2M, we examined the whole genome sequencing data in more detail. There were no single nucleotide variations in the *AR*. Yet, there was a genomic amplification of chromosome Xq12 that spanned the *AR* gene and enhancer located 650 kb upstream (**Figure 4A**)[8,12,13]. Since the amplification was present in PDX-167.2M, but not PDX-167.1R, it likely arose during the progression to metastatic CRPC. Amplifications of the *AR* gene and enhancer have recently been identified as prominent features of CRPC, associated with higher *AR* expression and resistance to AR-directed therapies [8,12,13].

So far, few patient-derived models have been reported with amplifications of the *AR* enhancer, so we further examined its significance in these matching PDXs. In testosterone-supplemented mice, *AR* mRNA levels were only slightly higher in PDX-167.2M versus PDX-167.1R. Yet, there was a striking increase in *AR* transcript levels in PDX-167.2M grafts from castrate mice (**Figure 4B**). Indeed, the *AR* was much more highly expressed in PDX-167.2M grafts from castrate mice compared to several other samples of prostate cancer, including 1) LNCaP cells grown in FBS; 2) other AR-positive PDXs, with diverse *AR* alterations, that were grown in either testosterone-supplemented or castrated mice; and 3) samples of patient metastases (**Figure 4B**). It is well known that castration stimulates *AR* mRNA expression in prostate cancer cells [38], and these

data show that it amplifies the difference in *AR* expression between PDX-167.1R and PDX-167.2M.

Androgens suppress *AR* mRNA expression but increase AR protein stability and nuclear translocation [38]. Therefore, we used immunohistochemistry to examine AR levels and localisation in PDX-167.1R and PDX-167.2M. In grafts from testosterone-supplemented mice, there was intense nuclear AR staining in both PDXs (**Figure 4C**). The pattern of staining was similar with an antibody raised to the AR N-terminus, which detects all forms of the AR, and an antibody raised to the AR C-terminus, which only detects full-length AR. In castrated mice, which have minimal levels of circulating androgens, intense nuclear AR staining was still observed in grafts from PDX-167.2M, as well as abundant cytoplasmic AR staining (**Figure 4C**). In castrated mice, PDX-167.2M also expressed increased levels of two AR splice variants, *ARV7* and *ARV9*, constitutively active forms of the AR that lack the ligand binding domain (**Figure 4C,D**) [39]. Gene set enrichment analyses showed slightly decreased enrichment scores for AR activity in PDX-167.2M in castrate mice compared to PDX-167.1R and PDX-167.2M in mice supplemented with testosterone (**Figure 4E and supplementary material, Figure S4**). Nevertheless, compared to other AR-positive PDXs, patient samples, and AR-null PDXs as controls, AR activity was sustained in PDX-167.2M in castrate mice. Thus, the amplification of the *AR* and enhancer in PDX-167.2M is associated with high AR expression and sustained AR activity under castrate conditions.

The AR amplification in PDX-167.2M is associated with resistance to AR-directed therapies

Amplifications of the *AR* and enhancer are associated with resistance to second generation AR-directed therapies [8,13,14]. Therefore, we examined the response of

PDX-167.2M, grown in castrate mice, to enzalutamide, and apalutamide. *In vivo*, PDX-167.2M was resistant to both treatments, with no significant decrease in overall tumour growth compared to the vehicle control across 4 weeks of treatment (**Figure 5A**). We also assessed the response of individual tumours to treatment using pre-defined thresholds for a good response (final tumour <100% of starting tumour volume), partial response (final tumour volume >100% of starting tumour volume but <50% of the average of the matched vehicle control) and no response (final tumour volume >50% of the average of the matched vehicle control). Based on these criteria, no tumours responded to enzalutamide or apalutamide treatment (**Figure 5B,C**). This is consistent with this patient's lack of response to enzalutamide in the clinic, approximately 8 months after the tissue for PDX-167.2M was obtained (**Figure 1D**).

We also examined the response of PDX-167.1R, which lacks the *AR* amplification, to AR-directed treatments. To measure acute responses to treatment, we grew PDX tissues as explants and organoids (**supplementary material, Figure S5A**). PDX-167.1R explants were sensitive to 48 hr treatments of both enzalutamide and apalutamide, with a significant decrease in the percentage of Ki67-positive cells (**supplementary material, Figure S5B,C**). There was also a significant decrease in the growth of PDX-167.1R organoids treated for four days with a dose response of enzalutamide (**supplementary material, Figure S5D**). In contrast, PDX-167.2M tissue was not sensitive to enzalutamide or apalutamide in explant or organoid experiments (**supplementary material, Figure S5B–D**), consistent with its responses *in vivo* (**Figure 5A–C**). Altogether, these data confirm that PDX-167.1R is sensitive to AR-directed treatments, but PDX-167.2M, which has an *AR* amplification, is resistant.

To examine the response of PDX-167.2M to other systemic treatments for advanced prostate cancer, we treated tumours with docetaxel, to represent taxane chemotherapy,

carboplatin, to represent platinum chemotherapy, and talazoparib, to represent PARP inhibitors. Overall, there was a significant average decrease in the growth of PDX-167.2M after docetaxel treatment compared to vehicle control, with one out of the seven tumours classified as a good responder due to tumour shrinkage across the treatment period (**Figure 5A–C**). This is consistent with the response of this patient to taxanes (cabazitaxel) approximately 3 months after the spinal metastasis was removed, despite previous chemo-hormonal therapy (**Figure 1D**). There was no change in the growth of PDX-167.2M after carboplatin or talazoparib treatment (**Figure 5A–C**), as expected given the lack of deleterious alterations in DNA damage repair genes (**supplementary material, Figure S2C**).

PDX-167.2M has a partial response to BET inhibition

We considered what other therapies might be effective for tumours with *AR* amplifications, and hypothesised that targeting transcription factors or chromatin regulators that bind to the *AR* enhancer may be one approach. We used Cistrome Data Browser to search publicly available chromatin immunoprecipitation (ChIP) datasets [40]. As shown previously, in addition to the AR itself, several lineage transcriptional activators, such as FOXA1, GATA2, HOXB13, and NKX3.1, bind to the DNase I hypersensitive site and surrounding region of the *AR* enhancer (**supplementary material, Figure 6A,B**); however, they are not readily druggable targets [13]. Nevertheless, this region is also bound by BRD4, a member of the bromodomain and extra-terminal domain (BET) family of epigenetic readers that bind to acetylated lysine residues in histones and are targeted by BET inhibitors. In 22Rv1 prostate cancer cells, BRD4 binding to the *AR* enhancer overlaps with peaks for the AR, histone 3 lysine 27 acetylation (H3K27ac), and Assay for Transposase-Accessible Chromatin (ATAC)

sequencing, confirming that there is open chromatin at this site (**supplementary material, Figure 6C,D**) [41-43]. BRD4 also binds to the *AR* promoter (**supplementary material, Figure 6D**). Notably, the BET inhibitor JQ1 decreased BRD4 binding at the *AR* enhancer and promoter (**supplementary material, Figure 6C,D**).

We therefore hypothesised that PDX-167.2M may be responsive to BET inhibition. To assess the *in vivo* response, PDXs were treated with the BET inhibitor ZEN-3694 for 28 days. Whilst overall there was no significant difference in tumour volume between control and treatment groups (**Figure 5A**), individual mice did have varying responses to ZEN-3694 treatment and 38% (3/8) of grafts were classified as good responders due to tumours shrinking in volume across the treatment period (**Figure 5B,C**). Thus, BET inhibition was more successful at decreasing tumour growth compared to both the AR-directed therapies enzalutamide and apalutamide, as well as talazoparib and carboplatin treatment.

Discussion

In 1941, Huggins and Hodges noted that “all known types of adult prostatic epithelium undergo atrophy when androgenic hormones are greatly reduced in amount or inactivated”, yet “it is certain that in many cases regression of the neoplasm is not complete” [44]. After 80 years, the same fundamental challenge remains; tumours inevitably acquire diverse mechanisms of resistance that sustain AR activity. Recently, the genomic mechanisms of resistance were traced beyond the *AR* locus to an upstream enhancer that is often amplified in CRPC [8,12,13]. Here we present PDXs of castrate-sensitive and castrate-resistant tumours from Patient 167, which acquired an amplification spanning the *AR* gene and enhancer during the progression to CRPC. These PDXs provide new models for studying this recently recognised form of castration resistance.

The transition from castrate-sensitive to castrate-resistant prostate cancer is a critical step in disease progression, so a collection of approaches is necessary to model it. Classical models include the C4-2 and C4-2B sublines from LNCaP cells, and the CWR series, which were generated by selecting cancer cells that metastasised or withstood castration in mice [45–48]. Different sublines of PDXs have also been established by growing them in castrated mice to select tumours with varying degrees of castrate-sensitivity and androgen-responsiveness [49–51]. An alternative approach, as taken in this study, is to establish patient-matched models from pre- and post-treatment samples [52]. The PDXs from Patient 167 provide isogenic models with and without an *AR* enhancer amplification and will enable preclinical studies of treatments that may overcome this mechanism of castration resistance. Other models with *AR* amplifications include the VCaP cell line and LNCaP cells with knock-in of the *AR* enhancer [13,53].

Given that *AR* enhancer amplifications are prevalent within patient samples, reanalysis of other previously established models of CRPC where the *AR* enhancer has not yet been examined is likely to uncover additional models of this form of castration-resistance.

The primary tumour from Patient 167 typifies the concept of prostate cancer “nimbosus” (gathering of stormy clouds), defined as the co-occurrence of multiple, adverse features in high-risk tumours [54]. This large volume tumour had grade group 5 adenocarcinoma with large cribriform architecture and IDC-P; two pathological features associated with increased risk of biochemical relapse and metastasis [54,55]. Sequencing of the primary tumour and PDX-167.1R showed high percent genome alteration, and loss of *PTEN* and *TP53*, which also portend poor prognosis [56]. Notably, these genomic alterations are more common in tumours with IDC-P or large cribriform architecture [57–59]. Biallelic *BRCA2* loss is also associated with IDC-P and cribriform architecture, but not in this instance [60]. Collectively, these morphological and molecular features suggest that the primary tumour from Patient 167 was highly likely to progress to advanced disease and require systemic treatments, making it a useful model of high-risk castrate-sensitive prostate cancer.

The development of metastatic CRPC in Patient 167 was associated with an amplification of chromosome X from the centromere through to the *AR*, with a further focal amplification of approximately 2,000 kb that spanned the *AR* gene and enhancer. Amplifications of the *AR* gene are well-known causes of castration resistance [10]. Recent studies have shown that amplifications often encompass an upstream *AR* enhancer that regulates *AR* expression [8,12], and sometimes there can be selective gain of the *AR* gene or enhancer [14,21,42]. Overall, *AR* amplifications have been

detected in 45–80% of patient samples with metastatic CRPC and are associated with increased *AR* mRNA abundance [8,12,14]. In PDX-167.2M, amplification of the *AR* and *AR* enhancer was associated with high *AR* expression, sustained AR signalling, and growth in castrated mice. Transcript and protein levels of full-length AR and AR-V7 in PDX-167.2M differed between testosterone-supplemented and castrated mice. The striking increase in *AR* mRNA abundance after castration was likely due to decreased auto-repression, because agonist-bound AR protein usually represses *AR* expression through a binding site in intron 2 [61]. In castrated mice, which have testosterone levels that approximate patients treated with abiraterone [37], there was abundant cytoplasmic AR staining, but still sufficient nuclear full-length AR and AR-V7 to sustain AR pathway activity. Further analysis of the correlations between *AR* amplifications, and the levels and localisation of full-length and variant forms of the AR, may refine the mechanisms of resistance to androgen-deprivation and AR-directed therapies.

AR amplifications have been associated with resistance to AR-directed therapies in cell lines and patients [8,13,14], and now in PDX-167.2M, which was resistant to enzalutamide and apalutamide *ex vivo* and *in vivo*. It is important to identify other treatments that overcome this mechanism of resistance. Since BRD4 binds to the *AR* enhancer, we used PDX-167.2M to investigate the efficacy of the BET inhibitor ZEN-3694. Notably, BET inhibitors have multiple effects in prostate cancer cells, such as down-regulating the expression of AR target genes, AR variants, and MYC [62-65]. BET inhibitors have been shown to suppress prostate cancer cell growth in preclinical models [62,63,65], and are currently undergoing clinical evaluation in patients with CRPC.

Here, we found that monotherapy with ZEN-3694 outperformed enzalutamide or apalutamide in decreasing the growth of PDX-167.2M, although it did not reduce the

volume of all grafts. The reason for the variability in graft response to BET inhibition is not clear; however, it suggests that combination therapies with BET inhibitors may be required to induce greater and more consistent decreases in tumour volume. One potential combination therapy is BET inhibition with enzalutamide. Indeed, a phase 1b/2a trial combined ZEN-3694 and enzalutamide for patients with CRPC who had previously failed an AR-directed therapy and showed that it was tolerable and had potential efficacy in some patients [66]. Intriguingly, patients in this trial with high AR activity scores (and possibly *AR* amplifications) in biopsies prior to treatment tended to progress more rapidly on combined treatment with ZEN-3694 and enzalutamide compared to those with low AR activity scores [66]. This could suggest that BET inhibitors modify the reliance of tumours on AR signalling in cases of low AR activity, or that tumours with high AR signalling scores are inherently aggressive. This highlights the challenge in treating tumours that are resistant to AR-directed inhibitors and demonstrates the importance of studying these treatments in the context of the AR pathway, including *AR* amplifications. Other combination therapies could be investigated and the matched PDXs established in this study will be useful for screening these potential treatments.

In conclusion, this study provides a novel matched pair of PDXs of castrate-sensitive and castrate-resistant prostate cancer. Disease progression of this high-risk case of prostate cancer was associated with common genomic alterations, including an *AR* gene and AR enhancer amplification. BET inhibition was more effective at decreasing tumour growth compared to AR-directed therapies; however, further work is required to identify therapies that target tumours with *AR* amplifications, including combinations with BET inhibitors. Overall, this work provides new models to study *AR* enhancer amplifications and overcome this newly recognized form of castration resistance.

Acknowledgements

We wish to acknowledge the people of the Kulin Nations; on whose land these studies were done. We pay our respects to their Elders, past and present. We thank the patients and families who generously supported this research by consenting to provide tissue; members of the Melbourne Urological Research Alliance (MURAL), Melissa Papargiris, and Jenna Kraska for providing PDXs; Wallace Crellin and James McPherson for invaluable advice; Melissa Bullock, William Jenkins, Shivakumar Keerthikumar, Samantha O'Dea, Michelle Richards, Linda Teng, and Hong Wang for laboratory assistance; Zenith Epigenetics for supplying ZEN-3694; and the Monash University Histology Platform, Monash University Animal Research Laboratories, Monash Biomedicine Discovery Institute Organoid Program, and Peter MacCallum Cancer Centre Molecular Genomics Core Facility for technical expertise. This work was supported by the National Health and Medical Research Council, Australia [fellowship 1102752 to G.P.R., project grants 1138242, 1121057, 1077799]; the Department of Health and Human Services acting through the Victorian Cancer Agency [fellowships MCRF18017 to M.G.L., MCRF15023 to R.A.T., MCRF17005 to D.L.G, CAPTIV Program]; the US Department of Defense through the Prostate Cancer Research Program [W81XWH1810349 to G.P.R.; opinions, interpretations, conclusions, and recommendations are those of the authors and are not necessarily endorsed by the Department of Defense]; the CASS Foundation [Medical Science grant 7139 to M.G.L.]; Monash University Faculty of Medicine, Nursing and Health Sciences [Bridging Post-doctoral Fellowship to LHP]; the Movember Foundation [Global Action Plan 1]; the Peter MacCallum Cancer Foundation [D.L.G]; the EJ Whitten Foundation; the Peter and Lyndy White Foundation; and TissuPath Pathology.

Author contributions statement

DLG, GPR, RAT, and MGL had full access to all the data in the study and take full responsibility for the integrity of the data and the accuracy of the data analysis.

Study concept and design: LHP, AB, DP, AC, DLP, GPR, RAT, MGL. Acquisition of data: LHP, AB, DP, AC, DC, JK, MGL. Analysis and interpretation of data: LHP, AB, AC, DLG, RAT, MGL. Drafting of the manuscript: LHP, AB, DGL, RAT, MGL. Critical revision of the manuscript for important intellectual content: LHP, AB, DP, AC, DC, JK, DLG, GPR, RAP, MGL. Statistical analysis: LHP, AB, MGL. Obtaining funding: DGL, GPR, RAT, MGL. Administrative, technical, or material support: MURAL. Supervision: DGL, GPR, RAT, MGL.

Data availability statement

DNA and RNA sequencing data are available from the Sequence Read Archive BioProject ID PRJNA681493. Patient-derived xenografts are available from the Melbourne Urological Research Alliance via an Expression of Interest.

References

1. Vander Griend DJ, Litvinov IV, Isaacs JT. Conversion of androgen receptor signaling from a growth suppressor in normal prostate epithelial cells to an oncogene in prostate cancer cells involves a gain of function in c-Myc regulation. *Int J Biol Sci* 2014; **10**: 627-642.
2. Pagliarini R, Shao W, Sellers WR. Oncogene addiction: pathways of therapeutic response, resistance, and road maps toward a cure. *EMBO Rep* 2015; **16**: 280-296.
3. Garraway LA, Sellers WR. Lineage dependency and lineage-survival oncogenes in human cancer. *Nat Rev Cancer* 2006; **6**: 593-602.
4. Crawford ED, Heidenreich A, Lawrentschuk N*, et al.* Androgen-targeted therapy in men with prostate cancer: evolving practice and future considerations. *Prostate Cancer Prostatic Dis* 2019; **22**: 24-38.
5. Bluemn EG, Coleman IM, Lucas JM*, et al.* Androgen receptor pathway-independent prostate cancer is sustained through FGF signaling. *Cancer Cell* 2017; **32**: 474-489.e476.
6. Beltran H, Prandi D, Mosquera JM*, et al.* Divergent clonal evolution of castration-resistant neuroendocrine prostate cancer. *Nat Med* 2016; **22**: 298.
7. Coutinho I, Day TK, Tilley WD*, et al.* Androgen receptor signaling in castration-resistant prostate cancer: a lesson in persistence. *Endocr Relat Cancer* 2016; **23**: T179-T197.
8. Viswanathan SR, Ha G, Hoff AM*, et al.* Structural Alterations Driving Castration-Resistant Prostate Cancer Revealed by Linked-Read Genome Sequencing. *Cell* 2018; **174**: 433-447 e419.
9. Chaturvedi AP, Dehm SM. Androgen Receptor Dependence. *Adv Exp Med Biol* 2019; **1210**: 333-350.
10. Visakorpi T, Hyytinen E, Koivisto P*, et al.* In vivo amplification of the androgen receptor gene and progression of human prostate cancer. *Nat Genet* 1995; **9**: 401-406.
11. Robinson D, Van Allen EM, Wu YM*, et al.* Integrative clinical genomics of advanced prostate cancer. *Cell* 2015; **161**: 1215-1228.

12. Quigley DA, Dang HX, Zhao SG*, et al.* Genomic hallmarks and structural variation in metastatic prostate cancer. *Cell* 2018; **174**: 758-769.e759.

13. Takeda DY, Spisák S, Seo J-H*, et al.* A somatically acquired enhancer of the androgen receptor is a noncoding driver in advanced prostate cancer. *Cell* 2018; **174**: 422-432.e413.

14. Dang HX, Chauhan PS, Ellis H*, et al.* Cell-free DNA alterations in the AR enhancer and locus predict resistance to AR-directed therapy in patients with metastatic prostate cancer. *JCO Precis Oncol* 2020; **4**: 680-713.

15. Tolmeijer SH, Boerrigter E, Schalken JA*, et al.* A Systematic Review and Meta-Analysis on the Predictive Value of Cell-Free DNA–Based Androgen Receptor Copy Number Gain in Patients With Castration-Resistant Prostate Cancer. *JCO Precision Oncology* 2020: 714-729.

16. Lawrence MG, Obinata D, Sandhu S*, et al.* Patient-derived models of abiraterone and enzalutamide-resistant prostate cancer reveal sensitivity to ribosome-directed therapy. *Eur Urol* 2018; **74**: 562-572.

17. Lawrence MG, Pook DW, Wang H*, et al.* Establishment of primary patient-derived xenografts of palliative TURP specimens to study castrate-resistant prostate cancer. *Prostate* 2015; **75**: 1475-1483.

18. Boeva V, Popova T, Bleakley K*, et al.* Control-FREEC: a tool for assessing copy number and allelic content using next-generation sequencing data. *Bioinformatics* 2012; **28**: 423-425.

19. Paradis E, Schliep K. ape 5.0: an environment for modern phylogenetics and evolutionary analyses in R. *Bioinformatics* 2019; **35**: 526-528.

20. Armenia J, Wankowicz SAM, Liu D*, et al.* The long tail of oncogenic drivers in prostate cancer. *Nat Genet* 2018; **50**: 645-651.

21. Wakefield LM. Xenomapper: Mapping reads in a mixed species context. *The Journal of Open Source Software* 2016; **1**.

22. Hanzelmann S, Castelo R, Guinney J. GSVA: gene set variation analysis for microarray and RNA-seq data. *BMC Bioinformatics* 2013; **14**: 7.

23. Hieronymus H, Lamb J, Ross KN*, et al.* Gene expression signature-based chemical genomic prediction identifies a novel class of HSP90 pathway modulators. *Cancer Cell* 2006; **10**: 321-330.

24. Nyquist MD, Corella A, Mohamad O*, et al.* Molecular determinants of response to high-dose androgen therapy in prostate cancer. *JCI Insight* 2019; **4**.

25. Nelson PS, Clegg N, Arnold H*, et al.* The program of androgen-responsive genes in neoplastic prostate epithelium. *Proc Natl Acad Sci U S A* 2002; **99**: 11890-11895.

26. Gillis JL, Selth LA, Centenera MM*, et al.* Constitutively-active androgen receptor variants function independently of the HSP90 chaperone but do not confer resistance to HSP90 inhibitors. *Oncotarget* 2013; **4**: 691-704.

27. Porter LH, Lawrence MG, Ilic D*, et al.* Systematic review links the prevalence of intraductal carcinoma of the rostate to prostate cancer risk categories. *Eur Urol* 2017; **72**: 492-495.

28. Sweeney CJ, Chen Y-H, Carducci M*, et al.* Chemohormonal therapy in metastatic hormone-sensitive prostate cancer. *N Engl J Med* 2015; **373**: 737-746.

29. James ND, Sydes MR, Clarke NW*, et al.* Addition of docetaxel, zoledronic acid, or both to first-line long-term hormone therapy in prostate cancer (STAMPEDE): Survival results from an adaptive, multiarm, multistage, platform randomised controlled trial. *The Lancet* 2016; **387**: 1163-1177.

30. Taylor RA, Fraser M, Livingstone J*, et al.* Germline *BRCA2* mutations drive prostate cancers with distinct evolutionary trajectories. *Nat Commun* 2017; **8**: 13671.

31. Williams JL, Greer PA, Squire JA. Recurrent copy number alterations in prostate cancer: an in silico meta-analysis of publicly available genomic data. *Cancer Genet* 2014; **207**: 474-488.

32. The Cancer Genome Atlas Research N. The molecular taxonomy of primary prostate cancer. *Cell* 2015; **163**: 1011-1025.

33. Fraser M, Sabelnykova VY, Yamaguchi TN*, et al.* Genomic hallmarks of localized, non-indolent prostate cancer. *Nature* 2017; **541**: 359-364.

34. Lalonde E, Ishkanian AS, Sykes J*, et al.* Tumour genomic and microenvironmental heterogeneity for integrated prediction of 5-year biochemical recurrence of prostate cancer: A retrospective cohort study. *The Lancet Oncology* 2014; **15**: 1521-1532.

35. Hieronymus H, Schultz N, Gopalan A*, et al.* Copy number alteration burden predicts prostate cancer relapse. *Proc Natl Acad Sci U S A* 2014; **111**: 11139-11144.

36. Soussi T, Kato S, Levy PP*, et al.* Reassessment of the TP53 mutation database in human disease by data mining with a library of TP53 missense mutations. *Hum Mutat* 2005; **25**: 6-17.

37. Michiel Sedelaar JP, Dalrymple SS, Isaacs JT. Of mice and men--warning: intact versus castrated adult male mice as xenograft hosts are equivalent to hypogonadal versus abiraterone treated aging human males, respectively. *Prostate* 2013; **73**: 1316-1325.

38. Burnstein KL. Regulation of androgen receptor levels: implications for prostate cancer progression and therapy. *J Cell Biochem* 2005; **95**: 657-669.

39. Luo J, Attard G, Balk SP*, et al.* Role of Androgen Receptor Variants in Prostate Cancer: Report from the 2017 Mission Androgen Receptor Variants Meeting. *Eur Urol* 2018; **73**: 715-723.

40. Zheng R, Wan C, Mei S*, et al.* Cistrome Data Browser: expanded datasets and new tools for gene regulatory analysis. *Nucleic Acids Res* 2019; **47**: D729-D735.

41. Cai L, Tsai YH, Wang P*, et al.* ZFX Mediates Non-canonical Oncogenic Functions of the Androgen Receptor Splice Variant 7 in Castrate-Resistant Prostate Cancer. *Mol Cell* 2018; **72**: 341-354 e346.

42. Consortium EP. An integrated encyclopedia of DNA elements in the human genome. *Nature* 2012; **489**: 57-74.

43. Chen Z, Wu D, Thomas-Ahner JM*, et al.* Diverse AR-V7 cistromes in castration-resistant prostate cancer are governed by HoxB13. *Proc Natl Acad Sci U S A* 2018; **115**: 6810-6815.

44. Huggins C, Stevens REJ, Hodges CV. Studies of prostatic cancer: II. The effects of castration on advanced carcinoma of the prostate gland. *Arch Surg* 1941; **43**: 209-223.

45. Thalmann GN, Sikes RA, Wu TT*, et al.* LNCaP progression model of human prostate cancer: androgen-independence and osseous metastasis. *Prostate* 2000; **44**: 91-103 Jul 101;144(102).

46. Sramkoski RM, Pretlow TG, 2nd, Giaconia JM*, et al.* A new human prostate carcinoma cell line, 22Rv1. *In Vitro Cell Dev Biol Anim* 1999; **35**: 403-409.

47. Thalmann GN, Anezinis PE, Chang SM*, et al.* Androgen-independent cancer progression and bone metastasis in the LNCaP model of human prostate cancer. *Cancer Res* 1994; **54**: 2577-2581.

48. Nagabhushan M, Miller CM, Pretlow TP*, et al.* CWR22: The first human prostate cancer xenograft with strongly androgen-dependent and relapsed strains both in vivo and in soft agar. *Cancer Res* 1996; **56**: 3042-3046.

49. Nguyen HM, Vessella RL, Morrissey C*, et al.* LuCaP prostate cancer patient-derived xenografts reflect the molecular heterogeneity of advanced disease an--d serve as models for evaluating cancer therapeutics. *The Prostate* 2017; **77**: 654-671.

50. Lin D, Wyatt AW, Xue H*, et al.* High fidelity patient-derived xenografts for accelerating prostate cancer discovery and drug development. *Cancer Res* 2014; **74**: 1272-1283.

51. Palanisamy N, Yang J, Shepherd PDA*, et al.* The MD Anderson Prostate Cancer Patient-derived Xenograft Series (MDA PCa PDX) Captures the Molecular Landscape of Prostate Cancer and Facilitates Marker-driven Therapy Development. *Clin Cancer Res* 2020; **26**: 4933-4946.

52. Kohli M, Wang L, Xie F*, et al.* Mutational Landscapes of Sequential Prostate Metastases and Matched Patient Derived Xenografts during Enzalutamide Therapy. *PLoS ONE* 2015; **10**: e0145176.

53. Liu W, Xie CC, Zhu Y*, et al.* Homozygous deletions and recurrent amplifications implicate new genes involved in prostate cancer. *Neoplasia* 2008; **10**: 897-907.

54. Chua MLK, Lo W, Pintilie M*, et al.* A prostate cancer "Nimbosus": Genomic instability and SChLAP1 dysregulation underpin aggression of intraductal and cribriform subpathologies. *Eur Urol* 2017; **72**: 665-674.

55. Lawrence MG, Porter LH, Clouston D*, et al.* Knowing what's growing: Why ductal and intraductal prostate cancer matter. *Sci Transl Med* 2020; **12**.

56. Hamid AA, Gray KP, Shaw G*, et al.* Compound Genomic Alterations of TP53, PTEN, and RB1 Tumor Suppressors in Localized and Metastatic Prostate Cancer. *Eur Urol* 2019; **76**: 89-97.

57. Bettendorf O, Schmidt H, Staebler A*, et al.* Chromosomal imbalances, loss of heterozygosity, and immunohistochemical expression of TP53, RB1, and PTEN in intraductal cancer, intraepithelial neoplasia, and invasive adenocarcinoma of the prostate. *Genes Chromosomes and Cancer* 2008; **47**: 565-572.

58. Böttcher R, Kweldam CF, Livingstone J*, et al.* Cribriform and intraductal prostate cancer are associated with increased genomic instability and distinct genomic alterations. *BMC Cancer* 2018; **18**: 8-8.

59. Elfandy H, Armenia J, Pederzoli F*, et al.* Genetic and Epigenetic Determinants of Aggressiveness in Cribriform Carcinoma of the Prostate. *Mol Cancer Res* 2019; **17**: 446-456.

60. Castro E, Salles DC, Lozano R*, et al.* Association between BRCA2 status and histologic variants (intraductal [IDC] and cribriform [CRIB] histology) in prostate cancer (PC). *J Clin Oncol* 2020; **38**: 5579-5579.

61. Cai C, He HH, Chen S*, et al.* Androgen receptor gene expression in prostate cancer is directly suppressed by the androgen receptor through recruitment of lysine-specific demethylase 1. *Cancer Cell* 2011; **20**: 457-471.

62. Asangani IA, Dommeti VL, Wang X*, et al.* Therapeutic targeting of BET bromodomain proteins in castration-resistant prostate cancer. *Nature* 2014; **510**: 278-282.

63. Faivre EJ, McDaniel KF, Albert DH*, et al.* Selective inhibition of the BD2 bromodomain of BET proteins in prostate cancer. *Nature* 2020; **578**: 306-310.

64. Kregel S, Malik R, Asangani IA*, et al.* Functional and Mechanistic Interrogation of BET Bromodomain Degraders for the Treatment of Metastatic Castration-resistant Prostate Cancer. *Clin Cancer Res* 2019; **25**: 4038-4048.

65. Welti J, Sharp A, Yuan W*, et al.* Targeting Bromodomain and Extra-Terminal (BET) Family Proteins in Castration-Resistant Prostate Cancer (CRPC). *Clin Cancer Res* 2018; **24**: 3149-3162.

66. Aggarwal RR, Schweizer MT, Nanus DM*, et al.* A Phase Ib/IIa Study of the Pan-BET Inhibitor ZEN-3694 in Combination with Enzalutamide in Patients with Metastatic Castration-resistant Prostate Cancer. *Clin Cancer Res* 2020; **26**: 5338-5347.

67. Lawrence MG, Taylor RA, Toivanen R*, et al.* A preclinical xenograft model of prostate cancer using human tumors. *Nat Protoc* 2013; **8**: 836-848.

68. Toivanen R, Berman DM, Wang H*, et al.* Brief report: A bioassay to identify primary human prostate cancer repopulating cells. *Stem Cells* 2011; **29**: 1310-1314.

69. Li H. Aligning sequence reads, clone sequences and assembly contigs with BWA-MEM. *arXiv:13033997 [q-bioGN]* 2013.

70. DePristo MA, Banks E, Poplin R*, et al.* A framework for variation discovery and genotyping using next-generation DNA sequencing data. *Nat Genet* 2011; **43**: 491-498.

71. Lawrence M, Huber W, Pages H*, et al.* Software for computing and annotating genomic ranges. *PLoS Comput Biol* 2013; **9**: e1003118.

72. Martin M. Cutadapt removes adapter sequences from high-throughput sequencing reads. *2011* 2011; **17**: 3.

73. Koboldt DC, Zhang Q, Larson DE*, et al.* VarScan 2: somatic mutation and copy number alteration discovery in cancer by exome sequencing. *Genome Res* 2012; **22**: 568-576.

74. Cibulskis K, Lawrence MS, Carter SL*, et al.* Sensitive detection of somatic point mutations in impure and heterogeneous cancer samples. *Nat Biotechnol* 2013; **31**: 213-219.

75. McLaren W, Gil L, Hunt SE*, et al.* The Ensembl Variant Effect Predictor. *Genome Biol* 2016; **17**: 122.

76. Karczewski KJ, Weisburd B, Thomas B*, et al.* The ExAC browser: displaying reference data information from over 60 000 exomes. *Nucleic Acids Res* 2017; **45**: D840-D845.

77. Vaser R, Adusumalli S, Leng SN*, et al.* SIFT missense predictions for genomes. *Nat Protoc* 2016; **11**: 1-9.

78. Adzhubei IA, Schmidt S, Peshkin L*, et al.* A method and server for predicting damaging missense mutations. *Nat Methods* 2010; **7**: 248-249.

79. Poplin R, Ruano-Rubio V, DePristo MA*, et al.* Scaling accurate genetic variant discovery to tens of thousands of samples. *bioRxiv* 2018: 201178. Not peer reviewed.

80. Landrum MJ, Lee JM, Benson M*, et al.* ClinVar: improving access to variant interpretations and supporting evidence. *Nucleic Acids Res* 2018; **46**: D1062-D1067.

81. Rentzsch P, Witten D, Cooper GM*, et al.* CADD: predicting the deleteriousness of variants throughout the human genome. *Nucleic Acids Res* 2019; **47**: D886-D894.

82. Shen R, Seshan VE. FACETS: allele-specific copy number and clonal heterogeneity analysis tool for high-throughput DNA sequencing. *Nucleic Acids Res* 2016; **44**: e131.

83. Cameron DL, Schroder J, Penington JS*, et al.* GRIDSS: sensitive and specific genomic rearrangement detection using positional de Bruijn graph assembly. *Genome Res* 2017; **27**: 2050-2060.

84. Cameron D, Dong R. StructuralVariantAnnotation: Variant annotations for structural variants. In. version 1.6.0. ed. (ed)^(eds): R package, 2020.

85. Liao Y, Smyth GK, Shi W. The R package Rsubread is easier, faster, cheaper and better for alignment and quantification of RNA sequencing reads. *Nucleic Acids Res* 2019; **47**: e47.

86. McCarthy DJ, Chen Y, Smyth GK. Differential expression analysis of multifactor RNA-Seq experiments with respect to biological variation. *Nucleic Acids Res* 2012; **40**: 4288-4297.

87. Okonechnikov K, Imai-Matsushima A, Paul L*, et al.* InFusion: Advancing Discovery of Fusion Genes and Chimeric Transcripts from Deep RNA-Sequencing Data. *PLoS ONE* 2016; **11**: e0167417.

88. Liberzon A, Birger C, Thorvaldsdóttir H*, et al.* The Molecular Signatures Database (MSigDB) hallmark gene set collection. *Cell Systems* 2015; **1**: 417-425.

89. Kwon MJ, Oh E, Lee S*, et al.* Identification of novel reference genes using multiplatform expression data and their validation for quantitative gene expression analysis. *PLoS ONE* 2009; **4**: e6162.

90. Hernandez-Segura A, Rubingh R, Demaria M. Identification of stable senescence-associated reference genes. *Aging Cell* 2019; **18**: e12911.

91. Porter LH, Hashimoto K, Lawrence MG*, et al.* Intraductal carcinoma of the prostate can evade androgen deprivation, with emergence of castrate-tolerant cells. *BJU Int* 2018; **121**: 971-978.

92. Toivanen R, Frydenberg M, Murphy D*, et al.* A preclinical xenograft model identifies castration-tolerant cancer-repopulating cells in localized prostate tumors. *Sci Transl Med* 2013; **5**: 187.

93. Tomayko MM, Reynolds CP. Determination of subcutaneous tumor size in athymic (nude) mice. *Cancer Chemother Pharmacol* 1989; **24**: 148-154.

94. Centenera MM, Gillis JL, Hanson AR*, et al.* Evidence for efficacy of new Hsp90 inhibitors revealed by *ex vivo* culture of human prostate tumors. *Clin Cancer Res* 2012; **18**: 3562-3570.

95. Centenera MM, Raj GV, Knudsen KE*, et al. Ex vivo* culture of human prostate tissue and drug development. *Nature Reviews Urology* 2013; **10**: 483.

96. Gao D, Vela I, Sboner A*, et al.* Organoid cultures derived from patients with advanced prostate cancer. *Cell* 2014; **159**: 176-187.

97. Kent WJ, Sugnet CW, Furey TS*, et al.* The human genome browser at UCSC. *Genome Res* 2002; **12**: 996-1006.

References 67 – 97 are cited only in the supplementary material.

Figure legends

Figure 1. Establishing new patient-matched models of castrate-sensitive and castrate-resistant prostate cancer. (**A**) Schematic showing the sites where tissue was collected from Patient 167. The radical prostatectomy specimen was sampled for PDX-167.1R. A dural metastasis of the spinal cord at the ninth thoracic vertebrae was sampled for PDX-167.2M. (**B**) A plot showing the growth trajectory of each PDX. Each data point represents a different generation with a ≥10-fold increase in tumour volume. PDX-167.2M grows more rapidly than PDX-167.1R based on a steeper curve and shorter time for each generation. (**C**) Heatmap summarising the histopathological features of PDX-167.1R and PDX-167.2M at generations 1 and 5 compared to the original tumour tissues. (**D**) The treatment timeline for Patient 167 showing serum PSA values and each treatment that the patient received between diagnosis and death from CRPC. The arrows show when samples were obtained for PDX-167.1R and PDX-167.2M.

Figure 2. Molecular changes between the matched PDXs are associated with advanced prostate cancer. (**A**) A three-dimensional model of the patient's prostate gland (light grey), index tumour (red; Gleason grade group 4-5) and non-index tumour (blue; Gleason grade group 2). Regions across the index tumour (IT), non-index tumour (NIT), a local metastasis in fatty tissue adjacent to the prostate (local met), and benign prostate tissue were sampled for low coverage whole genome sequencing. (**B**) A phylogenetic tree showing the relationships between samples based on copy number alterations from low coverage whole genome sequencing (average 3.75X coverage, min-max 2–5X coverage) and whole genome sequencing for PDX-167.2M (45X coverage). (**C**) Copy number alterations in each sample based on 250 kb bins with low coverage whole genome sequencing (gain, red; loss, blue). (**D**) Graph of the percentage genome alteration (PGA) in each sample. (**E**) Copy number profile of PDX-167.1R and PDX-167.2M, sampled at generation one, based on whole genome sequencing. Dotted line shows baseline ploidy. (**F**) Summary of key somatic alterations in generation one samples of PDX-167.1R and PDX-167.2M based on whole genome sequencing. Clonal copy number changes in genes reported in Armenia *et al* [20] and Robinson *et al* [11] and somatic nucleotide variations with an allele frequency of greater than 0.75 (high gain ≥6 copies, dark red; gain, red; heterozygous loss, blue; homozygous loss, dark blue;

missense mutation, grey; frameshift mutation, green). Half-filled squares indicate subclonal events with ≥50% cell fraction. Abbreviations: A, anterior; L, left; GG, Gleason grade; I, index tumour; N, non-index tumour; P, posterior; PGA, percent genome alteration; R, right.

Figure 3. Matched PDXs are castration-sensitive and castration-resistant respectively *in vivo*. (**A,B**) Graft volume (**A**) and the percentage of Ki67-positive cells (**B**) in PDX-167.1R grown sub-renally in control mice bearing testosterone implants (+T; blue) or established in mice bearing testosterone implants and then castrated (Cx; grey) for 3 to 19 days (*$P < 0.05$, ****$P < 0.0001$; unpaired *t* tests for +T versus Cx at each time point; *N* = 7-8 grafts per treatment group; data shown as mean ± SEM). (**C,D**) Graft volume (**C**) and the percentage of Ki67-positive cells (**D**) in PDX-167.2M grown sub-renally in +T (blue) or Cx (grey) mice for 3 to 28 days (****$P < 0.0001$; unpaired *t* tests for +T versus Cx at each time point; *N* = 7-8 grafts per treatment group; data shown as mean ± SEM). (**E**) Graft volume for PDX-167.1R (orange) and PDX-167.2M (green) grown subcutaneously. Grafts were established in mice bearing testosterone implants until graft volume reached 200 mm^3, at which point mice were castrated (*N* = 3 grafts/PDX; data shown as mean ± SEM). (**F**) Graft volume for PDX-167.2M grown subcutaneously in Cx mice for four generations of mice (Cx G1-4; *N* = 3-4 grafts/generation; data shown as mean ± SEM).

Figure 4. The acquisition of castration resistance in 167 is associated with an amplification of the *androgen receptor* (*AR*) gene and AR enhancer. (**A**) Schematic representation of chromosome Xq12, containing the *AR* gene and AR enhancer. Focal amplification was detected in PDX-167.2M (green), but not PDX-167.1R (orange). (**B**) Quantseq data for AR transcript abundance (cpm) in PDX-167.1R and PDX-167.2M compared to AR-positive (AR+) and AR-null (AR-) PDXs from the MURAL cohort, primary and metastatic patient samples and LNCaP cells grown in 5% FBS. PDXs were grown in mice supplemented with testosterone (+T) and castrated (Cx) mice. (**C**) Representative images of immunohistochemistry with antibodies directed to the AR N-terminus (AR-N), AR C-terminus (AR-C), or ARV7. Scale bar = 20 µm. (**D**) Plot of RT-qPCR data for full-length *AR*, *ARV7* and *ARV9* expression in PDX-167.1R, -167.2M (+T) and -167.2M (Cx). Data represent average relative expression (± SEM) relative to *AR*-

FL in LNCaP cells cultured in FBS (PDX-167.1R *N* = 3; PDX-167.2M *N* = 4; PDX-167.2M *N* = 1). (**E**) Boxplots of single-sample gene set enrichment analyses (ssGSEA) for the AR pathway from Hallmark 50 based on RNA sequencing in PDX-167.1R and PDX-167.2M compared to AR+ and AR- PDXs from the MURAL cohort, and primary and metastatic patient samples. PDXs were grown in +T and Cx mice.

Figure 5. The response of PDX-167.2M to systematic treatments for advanced prostate cancer. The *in vivo* treatment of PDX-167.2M with enzalutamide, apalutamide, docetaxel, carboplatin, talazoparib or ZEN-3694 compared to vehicle control for up to 28 days of treatment. (**A**) Graphs show tumour volume (mm^3) for PDXs treated with vehicle control (grey; *N* = 6 or 7 grafts) or drug (coloured; *N* = 5–8 grafts/treatment group). **P* < 0.05 compared to vehicle control; linear mixed model analyses. Data presented as mean ± SEM. (**B**) Graphs show percentage change in tumour volume from day 0 of treatment (%D0) for individual animals. Background colours show the range of tumour volumes classified as a good response (green; final tumour volume <100% of starting volume), partial response (yellow; final tumour volume >100% of starting volume but <50% of the average of the treatment-matched vehicle control) and no response (final tumour volume >50% of the average of the treatment-matched vehicle control), based on tumour volume at the end of the treatment period. (**C**) The percent of tumours classified as a good response (green), partial response (yellow) and no response (red) for each treatment group (*N* = 5–8 grafts/treatment group).

SUPPLEMENTARY MATERIAL ONLINE

Supplementary materials and methods

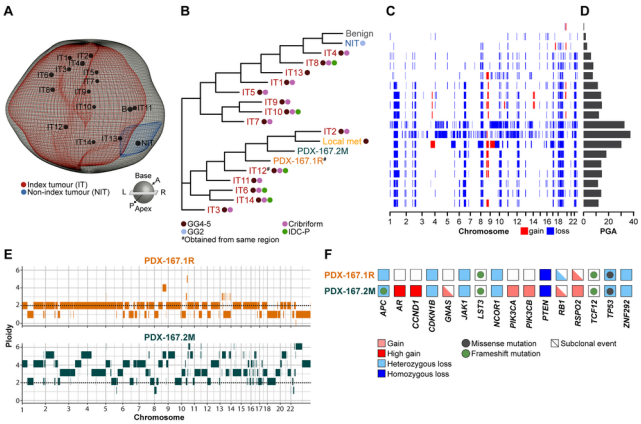

PATH_5652_Figure 2.tif

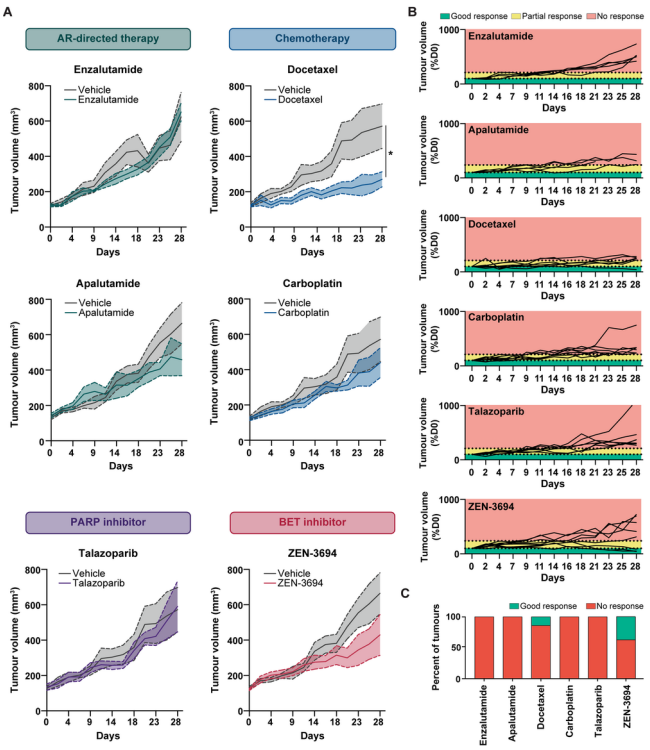

PATH_5652_Figure 5.tif

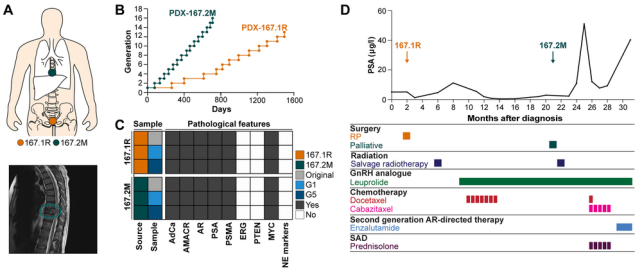

PATH_5652_Figure_1_RP.tif

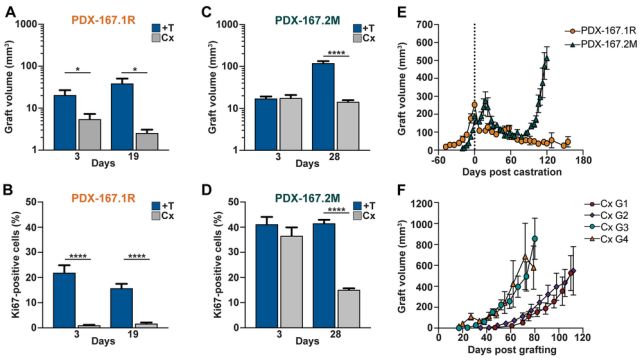

PATH_5652_Figure_3_RP.tif

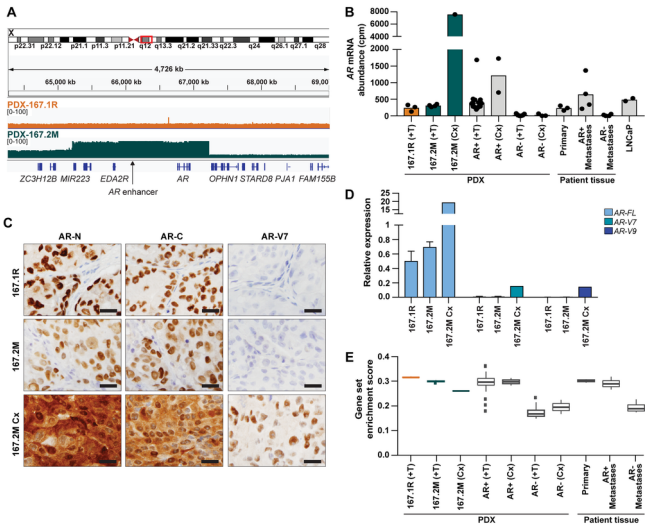

PATH_5652_Figure_4_RP.tif